Geothermics 64 (2016) 516–526

Contents lists available at ScienceDirect

Geothermics

journal homepage: www.elsevier.com/locate/geothermics

Exploring the shallow geothermal fluid reservoir of Fang geothermal system, Thailand via a 3-D magnetotelluric survey

Puwis Amatyakul[a], Songkhun Boonchaisuk[b], Tawat Rung-Arunwan[c], Chatchai Vachiratienchai[c], Spencer H. Wood[d], Kriangsak Pirarai[e], Aranya Fuangswasdi[e], Weerachai Siripunvaraporn[a,f,*]

[a] Department of Physics, Faculty of Science, Mahidol University, 272 Rama 6 Road, Rachatawee, Bangkok, 10400, Thailand
[b] Geoscience Program, Mahidol University, Kanchanaburi Campus, Saiyok, Kanchanaburi, Thailand
[c] Curl-E Geophysics Co., Ltd., 85/87 Nantawan Village, Uttayan-Aksa Road, Salaya, Phutthamonthon, Nakornpathom, 73170, Thailand
[d] Department of Geosciences, Boise State University, Boise, ID, 83701, USA
[e] Department of Groundwater Resources, Ministry of Natural Resources and Environment, 26/83 Soi Ngamwongwan 54, Ngamwongwan Road, Ladyao, Chatuchak, Bangkok, 10900, Thailand
[f] ThEP Center, Commission on Higher Education, 328, Si Ayutthaya Road, Rachatawee, Bangkok, Thailand

ARTICLE INFO

Article history:
Received 23 December 2015
Received in revised form 7 July 2016
Accepted 4 August 2016
Available online 10 August 2016

Keywords:
Thailand
Fang hot spring
Magnetotelluric
Geothermal

ABSTRACT

After early exploration during the 1980s and 1990s, the 0.3 MW Fang geothermal power plant was built as a demonstration to supply electricity to the local community. The shallow well (100 m) drilling program produced about 22 l/s of 125 °C water, and two wells to 500 m produced about 10 l/s. Due to the lack of detailed information on the geothermal system, the plan to expand to a larger power plant was halted to avoid the drilling missing the hot fluid. The plan was resumed in the last ten years starting with the magnetotelluric (MT) survey. Thirty three MT sites were deployed on the southern part of the Fang geothermal area. A remote site was installed about 600 km south of the study area for better data quality. After data processing, the data was inverted with WSINV3DMT to produce the 3-D resistivity model which clearly matches the near-surface geology and is also in agreement with the conceptual geology of the Fang geothermal system. The high resistivity zone is interpreted as the crystalline granitic rock, while the intermediate resistivity zone is associated with the Fang sedimentary basin. The resistivity contrast between the higher and lower resistivities helps reveal the orientations of the major Mae Chan Fault (MCF) and the two local faults of the area. The two main conductors of interests, C1 and C2, are directly linked to the hot fluid found at the surface. C1 is shallow (<50 m), and found only beneath the Fang hot spring, and so it is interpreted as the fracture reservoir. C2, which was not discovered in previous studies, extends from near the surface to a depth of 500 m, and at a depth of 200 m, it is about 1 km wide. It is about 1 km south of the Fang hot spring where the warm water was found to have seeped to the surface through the MCF. Two possible interpretations are proposed for the C2 conductor. The first is that there is an impermeable clay zone trapping a relatively high resistivity geothermal fluid reservoir beneath, like the caprock of a magmatic geothermal play type. This would require a deeper well to extract the hot fluid. As with the C1 conductor, the other interpretation is that the C2 conductor is a fracture geothermal reservoir where hot fluid from the deep resides within the pores of the sedimentary rock and fractures of the altered granite. This would require a shallower well. Both interpretations suggest that the C2 anomaly is of value. Since it has never been explored, a drilling over the C2 anomaly is recommended to probe its characteristic and also to extract more hot fluid for the future expansion of the geothermal power plant.

1. Introduction

The Fang geothermal area is about 140 km north of Chiang Mai city (Fig. 1). Evaluation of the area began in 1977 when detailed geological and resistivity surveys were conducted in the Fang hot springs area (rectangle in Fig. 1 and red dot in Fig. 2)

* Corresponding author at: Department of Physics, Faculty of Science, Mahidol University, 272 Rama 6 Road, Rachatawee, Bangkok, 10400, Thailand.
E-mail addresses: wsiripun@gmail.com, weerachai.sir@mahidol.ac.th (W. Siripunvaraporn).

http://dx.doi.org/10.1016/j.geothermics.2016.08.003
0375-6505/

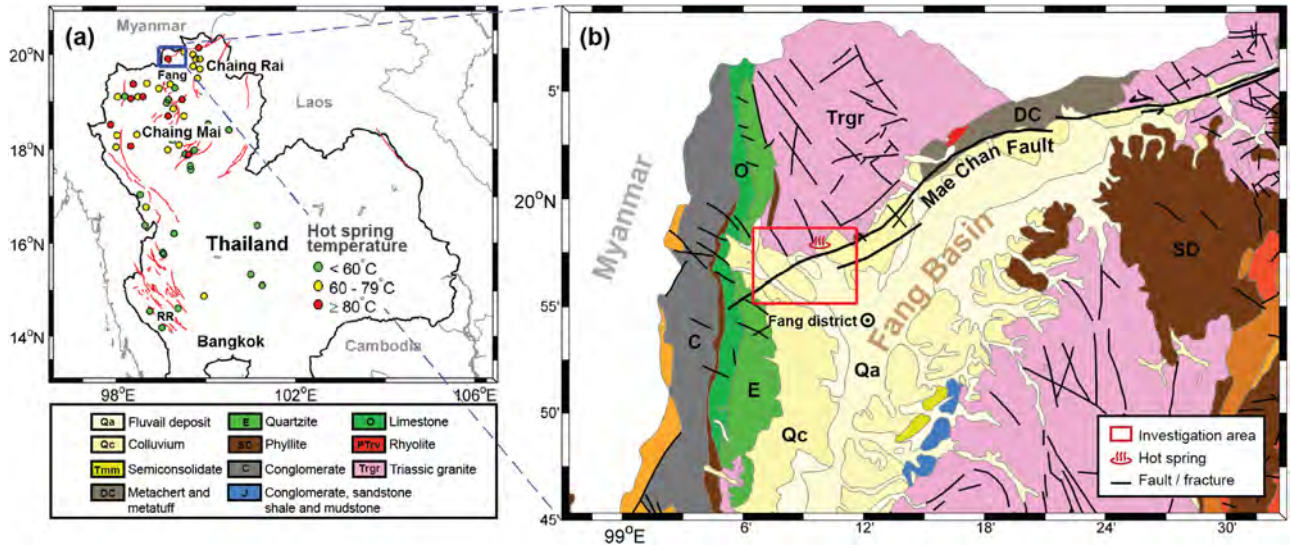

Fig. 1. (a) Hot springs in northern and western Thailand are marked as circles with different colors for different temperature ranges. The regional geology of the blue rectangle is shown in (b) in which the survey and study area of this paper is marked with a red rectangle. (For interpretation of the references to colour in this figure legend, the reader is referred to the web version of this article.)

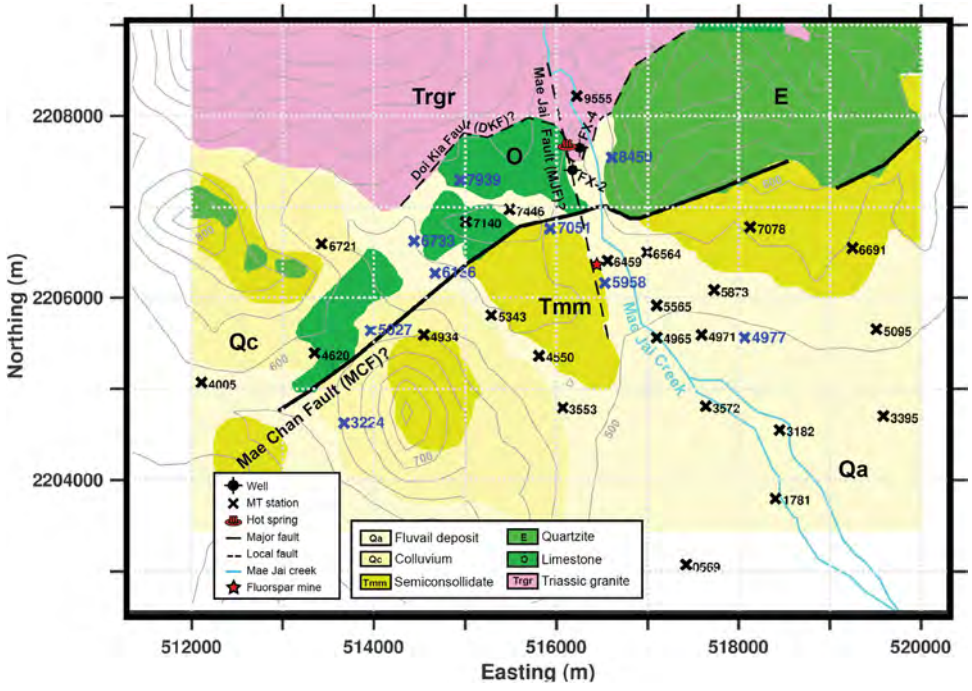

Fig. 2. Detailed geological rock units with major and local faults and topography of the Fang hot spring study area. The crosses indicate the MT sites. The observed data at the blue stations are shown in Figs. 4 and 5. DKF is the Doi Kia Fault; MJF is the Mae Jai Fault; MCF is the Mae Chan Fault drawn according to a recent survey by Wood (personal communication, 2015). FX-2 and FX-4 are the intermediate 500 m depth wells. (For interpretation of the references to colour in this figure legend, the reader is referred to the web version of this article.)

(Wanakasem and Takabut, 1986). Following the low resistivity zones (Coothongkul and Chinapongsanond, 1985), the shallow well (<100 m) drilling program around the hot spring yielded a flow of 22 l/s of 125 °C water (Ramingwong et al., 2000; Thienprasert et al., 1987). This flow rate was high enough to construct the 0.3 MW Fang demonstration geothermal power plant that has operated since 1988. It is currently the only geothermal power plant in Thailand.

Encouraged by the high temperature of the shallow wells, deep exploration was then continued in the 1990s in order to locate deeper reservoirs. In addition to the geological, electrical and geochemical surveys, four intermediate depth wells were drilled into the crystalline basement to a depth of 500 m. Two wells (Fx-2 and Fx-4 in Fig. 2) were successful in producing hot water at a temperature of 125–130 °C from the granite fractures at depths of around 270, 337 and 417 m (Korjedee, 2002; Ramingwong et al., 2000), while the other two were non-productive. The extracted hot water from these wells is currently used to generate electricity. All of the drilled holes were less than 200 m from the hot springs (Fig. 2). At the end of the feasibility studies, previous investigators have concluded that the deep drilling exploration has a very high risk of missing the target if a conventional vertical drilling technique is used (Korjedee, 2002; Ramingwong et al., 2000). It was concluded

that the hot geothermal fluid mostly resides within the narrow fractures of the steeply dipping faults. The geothermal project started in the 1980s was therefore not continued until recently.

The geothermal project at Fang was resumed in the 2010s. Studies by Owens (2012) again suggested that the electrical power plant of the Fang geothermal system could be upgraded from 0.3 MW to 2.8 MW. The idea is that the flow rate could be increased by putting pump installations in the existing wells and drilling new wells. To reduce the risk of deep drilling, a geophysical technique such as controlled source audio-magnetotelluric (CSAMT) method was recommended to help define the narrow fracture zones within the granite rocks (Singharajwarapan et al., 2012) and to image the geothermal system of the area for the first time. However, the CSAMT method requires an extra source to produce an electromagnetic wave making it more expensive than the traditional magnetotelluric (MT) method, and its investigation depths are typically less than 500 m which is less than our target depth. Funded by the Department of Groundwater Resource (DGR), Ministry of Natural Resources and Environment of Thailand, the audio-magnetotelluric (AMT) and magnetotelluric (MT) methods which are standard methods for geothermal exploration were therefore recommended for the investigation of the Fang geothermal system prior to further drilling and well-field design.

Geothermal systems have been classified into many types according to the geologic controls of the area (Moeck, 2014). Many MT experiments have been conducted over very high temperature geothermal systems which were mostly of the magmatic play type according to the classification of Moeck (2014). They found that the resistivity structure consists of a thin, conductive layer corresponding to clay-rich rocks acting as low-permeability caprock on top of a relatively higher resistivity geothermal reservoir where the hot fluids reside (e.g., Gasperikova et al., 2015; Heise et al., 2008; Pritchett, 2004; Pellerin et al., 1996; Rosenkjaer et al., 2015; Uchida and Sasaki, 2006).

The Fang geothermal system is a relatively low temperature system. It was classified in the IFC-IGA report (IFC-IGA, 2014) as being of an extinct magmatic play type controlled by batholiths without associated volcanism or a plutonic play type if using the catalog of Moeck (2014). The Fang conceptual model by Takashima and Kawada (1981), Takashima and Jarach (1987), Geotermica Italiana SRI (1984), Praserdvigai (1986) and Raksaskulwong (2008) shown in Fig. 3 proposed that a deep hot igneous body heats the trapped groundwater at greater depths to form a high temperature, deep geothermal reservoir. The hot fluid then rises up along the fractures of the fault zones to mix with the colder groundwater coming from above producing the geochemical equilibrium mixture of hot fluid with a temperature up to 160 °C. At shallower depths, the hot fluid is then stored along the fractures of the faults or within the weathered and altered granite rocks and the permeable sediments to form a shallower and lower temperature geothermal reservoir. Some of the hot fluid then continues ascending through the fault fractures to the surface in the form of hot springs.

According to the proposed conceptual model (Fig. 3), the results of MT surveys over the Fang geothermal system may produce a different resistivity structure from the conventional interpretation of magmatic types. The batholith heat source would likely be "mapped" as a high resistivity body, while the weathered rocks and permeable sediment filled with fluid would have a moderate resistivity. The hot fluid reservoir along the fractures of the fault might be "seen" directly as a conductive zone. The possibility of mapping the conductive clay caprock as in the magmatic play type is raised. One of our objectives of conducting the AMT and MT surveys over the Fang area is therefore to verify and validate the proposed conceptual model in Fig. 3 and to probe these major components of the Fang system. Location and size, particularly of the shallow hot fluid reservoir, will be useful for the assessment of the capability of the Fang geothermal system to expand its power production. We start the paper with the geology of the Fang hot spring. The AMT and MT data acquisition, data processing and inversion are described next. The interpretation to relate the inverted 3-D resistivity model with the previously proposed geothermal system is then discussed, followed by the conclusion.

2. Geology of the Fang hot spring

The Tertiary Fang basin is oriented NNE-SSW and is 50 km long and 20 km at the central widest part (Fig. 1). The Mae Chan fault (MCF) forms the NW boundary and separates the crystalline rocks on the north from the sediments of the basin. The MCF extends 150 km SW from the Thai–Lao border on the east to its termination in the Fang Basin (Fenton et al., 2003; Uttamo et al., 2003; Kosuwan and Lumjuan, 1998). The west end terminates against a N-S trending belt of west-dipping folded Paleozoic sediment. The Paleozoic belt is not offset by the fault, and motion must be taken up by N-S-trending western boundary faults of the Fang Basin. East of the Fang basin, the MCF exhibits an active left-lateral strike-slip offset (Fenton et al., 2003; Kosuwan and Lumjuan, 1998). Its left lateral motion implies that the SE block is pulling away from the N-S western boundary fault, and this may be the cause of permeable openings in the vicinity of the hot springs. Several hot springs emanate from along the MCF (Wood and Singharajwarapan, 2014) including the Fang hot spring. 40 km east of Fang is another prominent geothermal system, the Mae Chan hot spring studied by Amatyakul et al. (2015).

Fig. 2 summarizes the geology of the Fang Hot Springs. The hot springs and hot wells are in crystalline rocks comprised of gneissic granite and mylonite. The Age of the rocks and mylonitization is uncertain because no zircon ages have been obtained. Past studies have labeled these crystalline rocks as Carboniferous, and some studies have labeled the rocks as Triassic. Overlying the crystalline rocks are folded quartzose sandstone, quartzite, and lesser amounts of limestone and shale. Imsamut and Krawchan (2005) considered these sediments to be a part of the Mae Tha Group of late Carboniferous age.

The contact between crystalline rocks and the quartz sandstone dips gently (~12°) to the southeast and is considered to be a low-angle detachment fault and was called the Doi Kia Fault (DKF) by Chaturongkawanich et al. (1980) and is shown in Fig. 2. The crystalline rocks and the overlying Paleozoic sediment detachment are faulted down to the southeast along the high–angle MCF which appears here to have a large vertical displacement. The downthrown southeast block of the MCF is comprised of Cenozoic basin-fill sediment overlying Paleozoic quartzite. Petroleum exploration wells 4 km southeast of the fault were drilled to a depth of 772 m in this sediment resting on a "quartzite basement".

The Fang Hot Springs do not directly emanate from the trace of the MFC. Instead they flow from crystalline rock north of the fault. We observe that the hottest seeps (>90 °C) align along a 350–355° (N – NW) alignment for a distance of 100 m. One of the successful 500-m-deep wells is along this alignment 200 m south of the seeps. This N – NW trend is parallel to the linear stream valley of the Mae Chai creek (written as Mae Jai creek in Fig. 2). Previous investigators have assumed this lineament controls the fracture system of the hot springs. The fault is not observed in the stream valley, although bedrock exposure is good north of the hot springs. Shawe (1984) noted a fault of this orientation, with horizontal grooves and slickensides on the fault plane, in the open pit of the Huai Sai Fluorspar Mine (Fig. 2). He also noted warm springs at the southeast end of the pit. The mine pit, 1 km south of the 500-m well, is now a pond and cannot be examined. We use the name "Mae Jai fault (MJF)" for this N – NW feature, but its understanding awaits

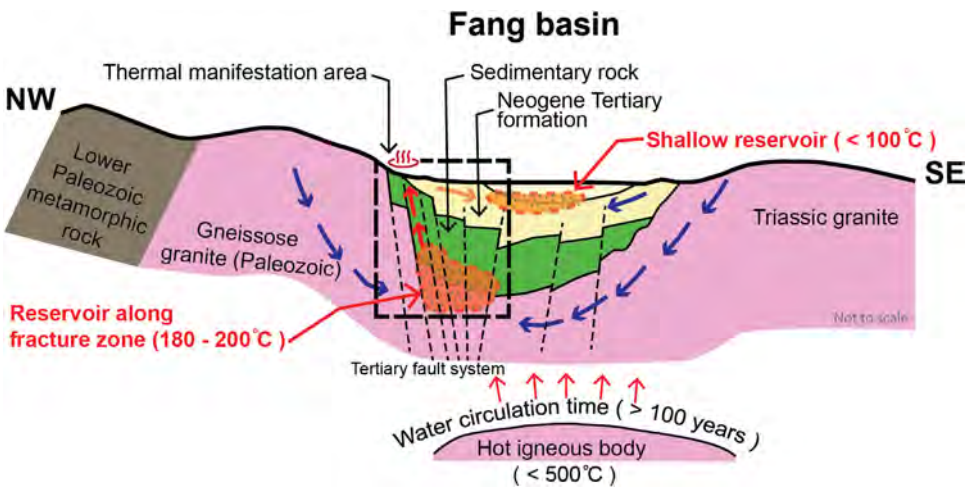

Fig. 3. The conceptual geothermal system of Fang hot spring redrawn after Takashima and Kawada (1981) and Takashima and Jarach (1987). The Black rectangle marks the area of our investigation.

more detailed mapping. Note: the name "Mae Chai" appears on the 1:50,000 topographic map 4848IV, but we use a spelling closer to the Thai pronunciation: "Mae Jai" to avoid confusion with the similar sounding Mae Chan fault.

3. Magnetotelluric survey

3.1. Data acquisition and data processing

In December 2014, 33 MT stations were deployed to cover the 6 km × 8 km area of interest surrounding the Fang Hot Springs (Fig. 2). Since local communities are distributed in the area, the site was designed according to the accessibility of land. The site spacing between stations is 500 m on average. The northern part of the Fang hot spring is inaccessible as it belongs to the Doi Pha Hom Pok national park. Most of the sites are therefore located within the sedimentary basin which is easy to access, whereas only a few sites are located on granite, limestone and sandstone rocks. Four sets of MT equipment that record the electric fields in the *x*- and *y*-directions (Ex and Ey) and the magnetic fields in the *x*-, *y*- and *z*-directions (Hx, Hy and Hz) were deployed overnight at four locations for about 20 h in order to acquire broadband data up to 1000s, where *x* is oriented north, *y* is oriented east and *z* is vertically downward. These four sets of equipment were then moved to acquire data at other locations shown in Fig. 2 for the total of 33 stations. Coils, magnetometers and data acquisition units are from KMS Technologies – KJT Enterprises Inc., Houston, Texas. To improve the data quality, another set of equipment was set up about 600 km south of the study area in Kanchanaburi province (Fig. 1) as a remote reference site. The data from the four local sites was then processed with the data from the remote site using KMS processing software based on the robust multiple-station technique of Egbert (1997).

For high frequency magnetic fields (>1000 Hz), high-frequency coils replaced the broadband magnetic coils to acquire the high frequency data for less than 30 min in each site. As we have only two sets of high-frequency coils, two local sites can therefore be acquired simultaneously. The two local sites then become a remote site for each other. However, as both are not too far from each other (less than 2–4 km), the data quality is not greatly improved.

After the data processing (Egbert, 1997), the high frequency band and broadband data were merged together. The very high frequency (>3000 Hz) and the very long period (>300 s) data are of much poorer data quality and were therefore removed. This leaves us the data (impedance tensor **Z** and the vertical magnetic transfer function **T**) from a period of 3000 Hz to 300 s for each site. To proceed to the inversion part, about 16 periods per site of the data were chosen at regular intervals on a $\log_{10}$ scale in this frequency range. Although the impedance tensor Z was used in the inversion, here, for simplicity, we instead plot the apparent resistivity and phase of the *xy*- and *yx*-modes with the error bars for some selected stations in Fig. 4 and the vertical magnetic transfer function or tipper in Fig. 5. Most of the on-diagonal data is severely contaminated by local noise and will be discarded for the inversion.

3.2. Three-dimensional inversion and the inverted model

The 16 periods off-diagonal impedance tensors and the tippers of all sites with the minimum error floor for both data sets at 5% are included for the 3-D inversion using the WSINV3DMT parallel version (Siripunvaraporn and Egbert, 2009; Siripunvaraporn et al., 2005). The inverse model was discretized using a 60 × 60 × 55 grid (with air layers on top of the topography) in the north-south, west-east and vertical directions, respectively. The grid spacing within the study area (Fig. 2) for the horizontal direction is 100 m. To avoid the boundary effects, the grid spacing is then increased in a logarithmic scale in both directions. In the vertical direction, the grid of the first layer was discretized finely enough to provide very high accuracy responses for all periods where the size of each subsequent layer is 1.2–1.8 times that of the previous layer. The accuracy of this discretized grid was tested with various half-space resistivity values from 1 to 1000 Ω m, and was shown to have less than 1% error, which is also less than the minimum error floors setting for the data. The workflow to obtain the final 3-D resistivity model is analogous to those presented in both Amatyakul et al. (2015) and Lindsey and Newman (2015) where coarse structures are recovered first followed by further sequential refinements performed here by adjusting the inversion parameters. The inversion was run with different initial models from a 10 Ω m half-space to 1000 Ω m half-space with a large smoothing factor. The inverted model from the initial half-space of 300 Ω m fits the data better. It was then selected as a starting and reference model for re-inversion with a smaller smoothing factor. At the end, we obtained a preferred inverted model that yields an acceptable RMS of 2.1 and fits well with the geology of the area. The observed data and calculated responses of some selected stations are plotted in Figs. 4 and 5.

The final inverted resistivity model is displayed in top view in Fig. 6 and in cross-sectional views perpendicular to the MCF in Fig. 7. It consists of four main structures which will be interpreted in the

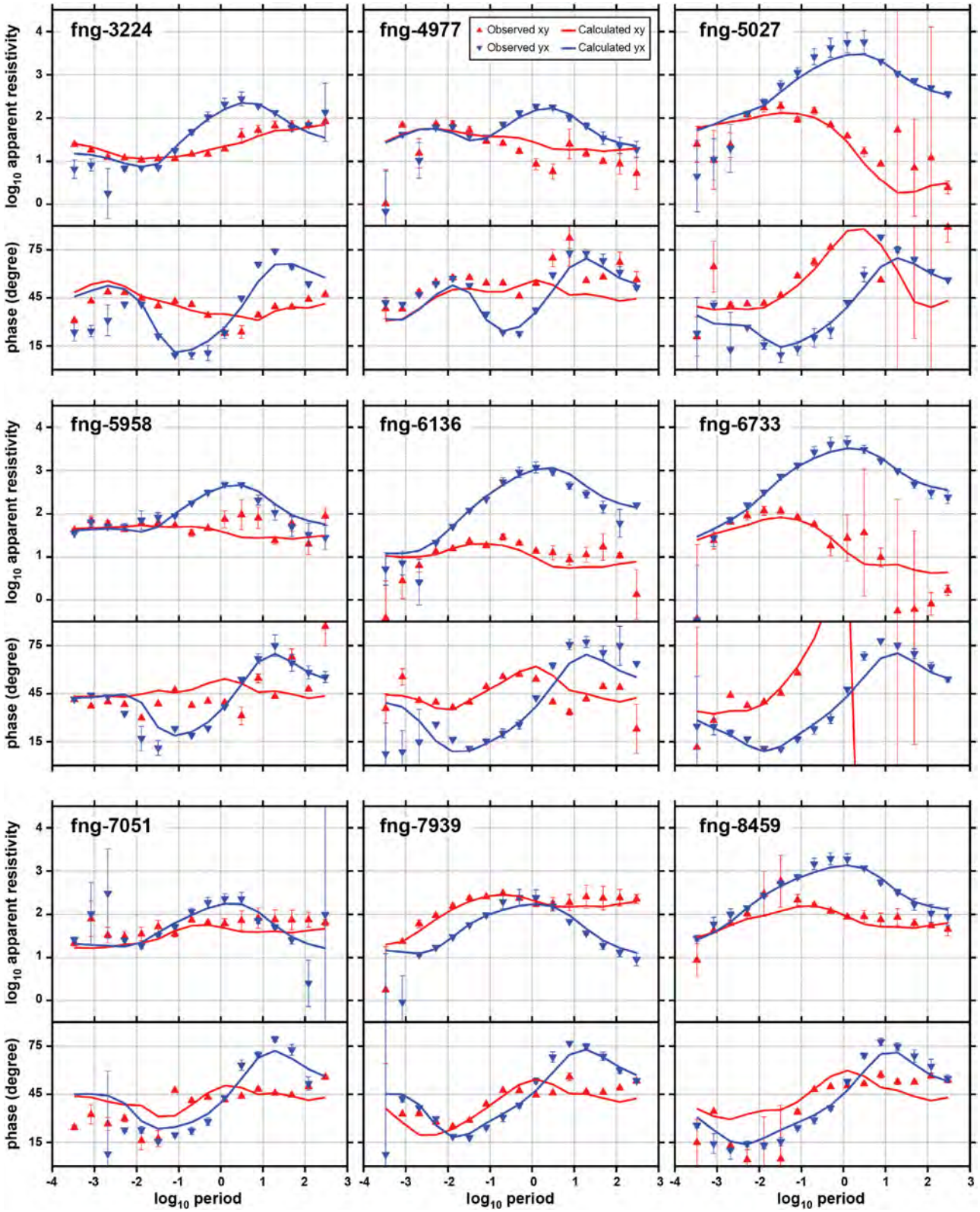

Fig. 4. Selected apparent resistivities (ohm-m) and phases (degree) as a function of $\log_{10}$ periods (second) computed from the off-diagonal impedance tensor at various locations acquired in the locations marked as blue crosses in Fig. 2. Red is xy and blue is yx mode. The "upward" and "downward" triangles and error bars are from field measurement, and the solid lines are the calculated responses generated from the inverted model shown in Figs. 6 and 7. (For interpretation of the references to colour in this figure legend, the reader is referred to the web version of this article.)

next section. (1) The high resistivity structure labeled as R (in blue in Figs. 6 and 7), where the resistivity is greater than 300 Ω m, appears mostly in the northern part of the study area before propagating southeastward at greater depths. (2) The moderate resistivity structure marked as M (in yellow and green in Figs. 6 and 7), where the resistivity is around 30–300 Ω m, is mostly in the southern

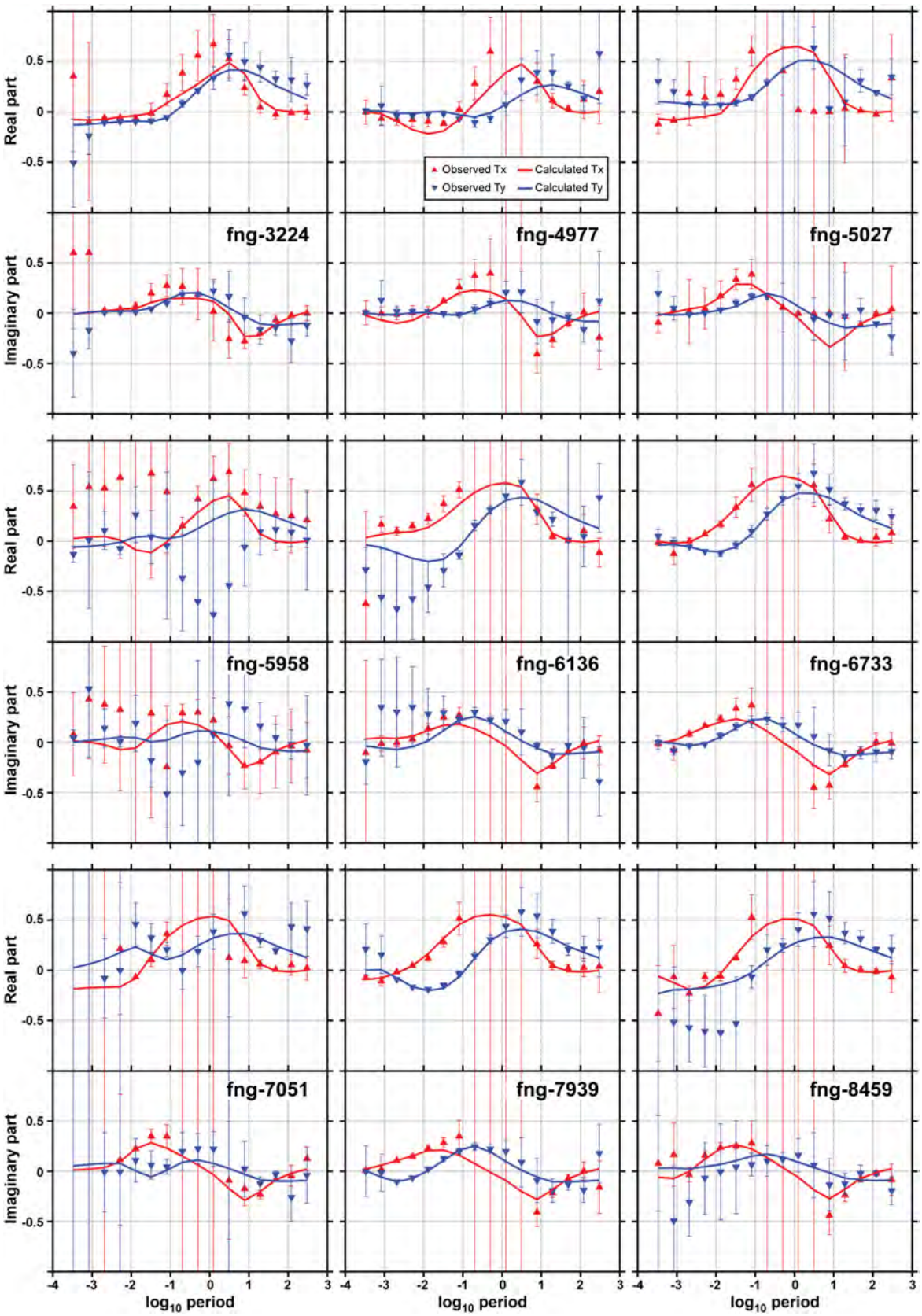

Fig. 5. Real and imaginary parts of vertical magnetic transfer functions (tipper) as a function of $\log_{10}$ periods (second) at various locations acquired in the locations marked as blue crosses in Fig. 2. Red is zx and blue is zy mode. The "upward" and "downward" triangles and error bars are from field measurement, and the solid lines are the calculated responses generated from the inverted model shown in Figs. 6 and 7. (For interpretation of the references to colour in this figure legend, the reader is referred to the web version of this article.)

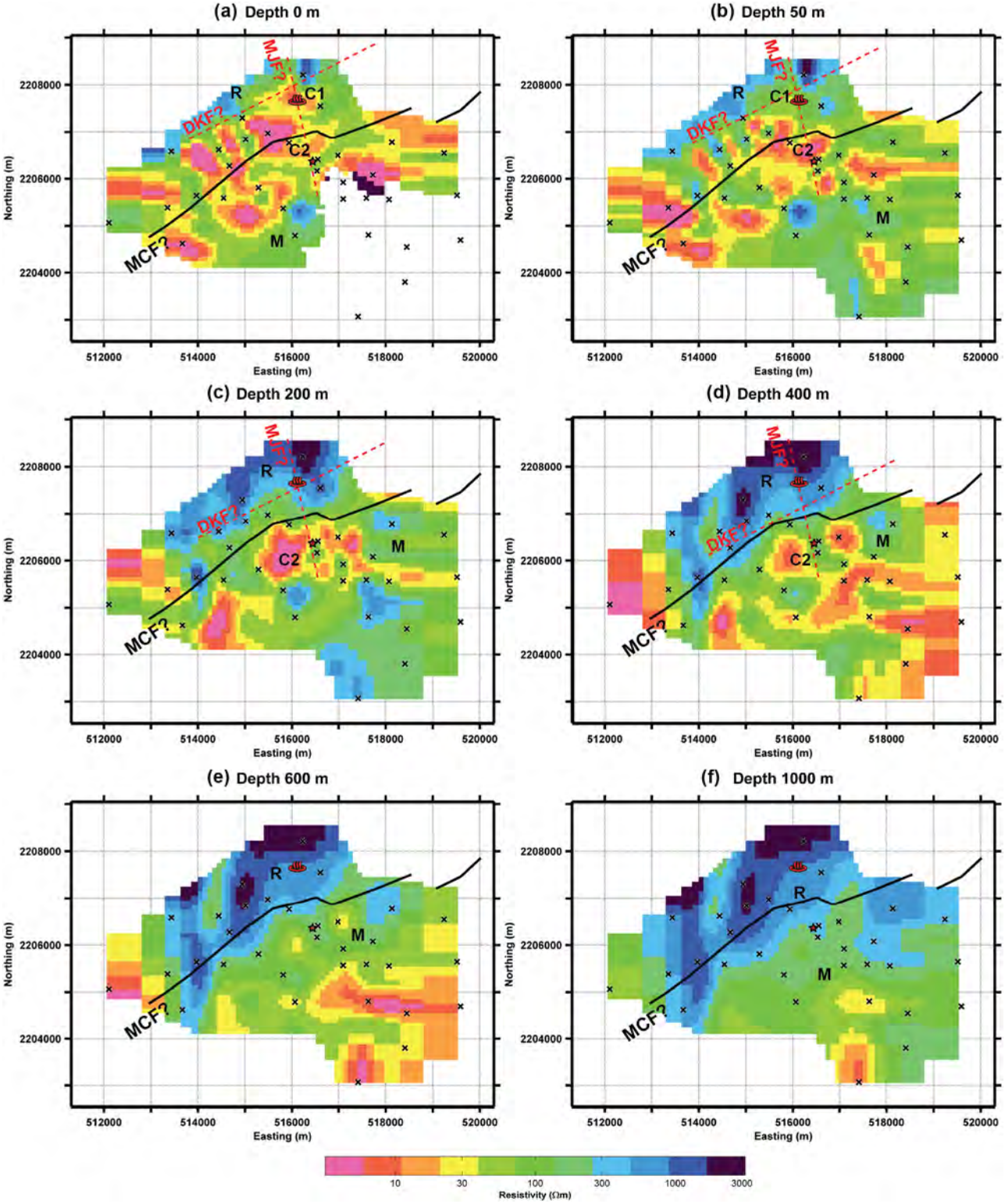

Fig. 6. The plane-view of the final inverted model shown as horizontal slices at (a) surface, depths of (b) 50 m, (c) 200 m, (d) 400 m, (e) 600 m, and (f) 1000 m. MT locations are marked as crosses (for the station names, refer to Fig. 2). MCF is the Mae Chan Fault based on the surface trace. The local faults are drawn in red dashed straight lines based on the observed resistivity contrasts, in which they also change with depth. R is the high resistivity zone associated with the granite rock, while M is for the lower resistivity zone corresponding to the sedimentary rock of the Fang basin. C1 and C2 are the two low resistivity zones expected to be hot geothermal reservoirs. (For interpretation of the references to colour in this figure legend, the reader is referred to the web version of this article.)

part and at shallow depth in the study area. At greater depth, it is replaced with the high resistivity structure. (3) The resistivity contrasts between both structures can be observed at shallower depth to great depth. These resistivity contrasts seem to be associated with the presence of the major and minor faults in the area.

(4) Although there are many conductive anomalies distributed throughout the study areas, we are solely interested in just the two

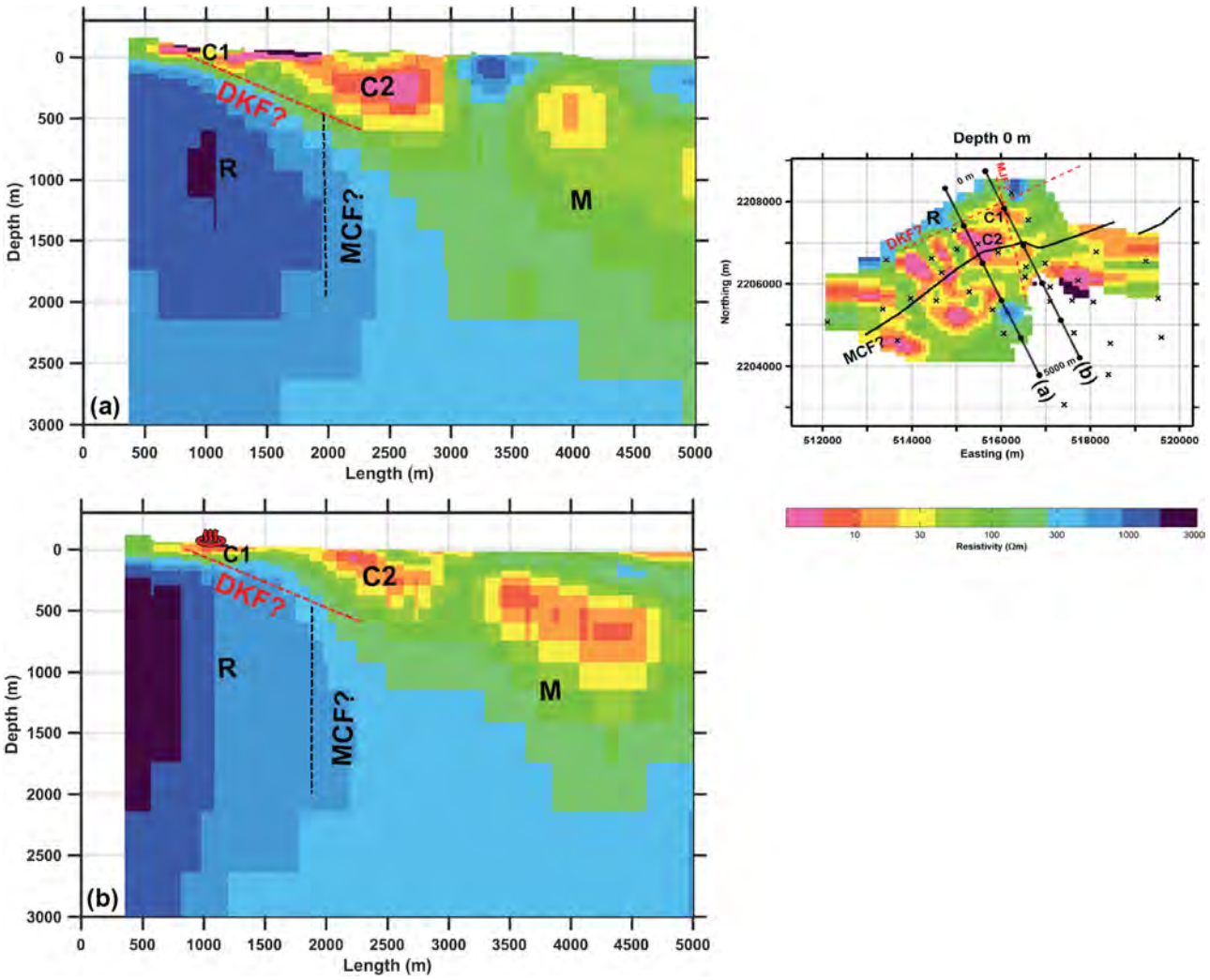

Fig. 7. (a) and (b) are cross-sectional plots of the final inverted model (Fig. 6) from northwest to southeast perpendicular to the Mae Chan Fault (MCF) and the Doi Kia Fault (DKF) where (b) cuts through the Fang hot spring and (a) is about 1 km south of (b). The red dashed lines are the estimated orientation of the DKF. The black dashed line shows the orientation of the MCF. (For interpretation of the references to colour in this figure legend, the reader is referred to the web version of this article.)

conductive anomalies (where the resistivity is lower than 30 Ω m) located around the middle of the study area labeled as C1 and C2 (Figs. 6 and 7) since there is direct evidence of hot fluid found in the areas of these two conductors, and no hot fluid found in the area of the other conductors. Conductor C1 is located in the vicinity of the Fang hot spring zone but appears only within the upper 50 m. Conductor C2 is about 1 km south of the hot spring and can be seen from near the surface to a depth of 500 m. Its width decreases and its resistivity increases with depth.

As conductor C1 and C2 are important and will be mentioned numerous times in the next section, it is better to verify their existence. To validate the conductors C1 and C2 in Figs. 6 and 7, we replaced C1 first with the neighboring resistivity values (between 100–300 Ω m) to simulate the case that C1 does not exist. We then ran the forward modeling to fit the observed data. The relative changes of the RMS values were calculated via

$$\text{Relative Change} = 100\% \times (\text{RMS}_{\text{new}} - \text{RMS}_{\text{original}})/\text{RMS}_{\text{original}},$$

for each station and plotted in Fig. 7, where RMS_{new} is the fit to the data after replacing the conductor with the neighboring resistivity, and $\text{RMS}_{\text{original}}$ is the RMS value from the inverted model of Fig. 6. By replacing the conductor C1 with the neighboring resistivity, the overall RMS increases from 2.1 to 2.6 (a 24% increase) indicating that the observed data really requires the C1 conductor. The relative change of RMS misfit at each site (Fig. 8a) shows that the misfits at the stations in the surrounding area of C1 change significantly certifying that C1 is needed by these stations.

A similar experiment is performed for the C2 conductor. We found that the overall RMS increases from 2.1 to 2.3 (a 9.5% increase). The overall change of RMS for C2 is less than that for C1. This is because C2 is deeper and smaller in size with a result that contribution from C2 is much less than from C1. Fig. 8b shows that the misfits of the stations in the surrounding area of C2 change dramatically after replacing C2 with neighboring resistivities. Both of these experiments (Fig. 8) confirmed that both conductors are required by the data and are not artifacts from the inversion.

4. Interpretation and discussion

Our inverted resistivity model (Figs. 6 and 7) is consistent with the surface geology of Fig. 2. By matching the surface resistivity (Fig. 6a) to the surface geology (Fig. 2), the high resistivity (R) zone in the northwest (in blue in Fig. 6a) is in agreement with the granite rock (Fig. 2). The lower resistivity zone (M) covering the southwestern part of the area (in yellow and green in Fig. 6a) corresponds to the Fang sedimentary basin in Fig. 2. The resistivity contrast between the high zone and low zone in the north matches well with

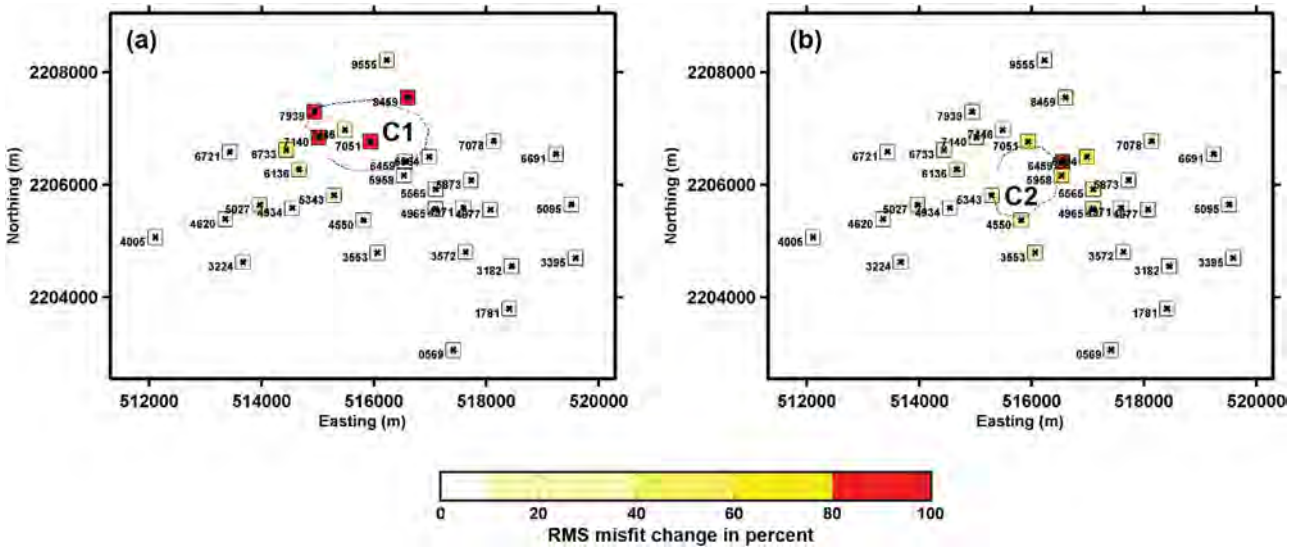

Fig. 8. Plots of relative change of RMS misfit between the observed data and the calculated data of each station (a) after replacing the C1 conductor of the inverted model (Figs. 6 and 7) with the neighboring resistivities and (b) after replacing the C2 conductor with the neighboring resistivities.

the surface trace of the Doi Kia Fault (DKF). Similarly, the resistivity contrast at the end of the thin conductive C1 zone in the northeast of the area appears to be consistent with the presence of the Mae Jai Fault (MJF). In Fig. 6a, for simplicity we represent the resistivity contrasts associated with both faults as straight lines instead of the actual surface trace as in Fig. 2. The intersection of both resistivity contrasts in the north encloses the high conductor C1 where its location corresponds to the position of the Fang hot spring (Figs. 6a and 2).

To infer the deeper structures, we assume that the same structures observed at the surface continue to greater depths. At depth (Fig. 6b–f), the resistive granite rock R showing in the northwest at the surface (Fig. 6a) appears in the southeast (Fig. 6b–f) and terminates at a depth of 600 m when it encounters the MCF. At depths below 2 km (Fig. 7), the study area overlies a high resistivity zone indicating the granite rocks lie beneath. It also indicates that the Fang basin has a thickness of around 2 km in this area. In earlier studies, geologists proposed that the possible heat sources of the Fang geothermal system are either a deep hot (>300 °C) igneous body or the radiogenic heat from the granite rock or both (Takashima and Kawada, 1981; Takashima and Jarach 1987). As our investigation depth is within the upper crust, one possible source of heat, the batholith granite lying beneath, is clearly imaged in this study (Fig. 7).

At the surface, the DKF separates the resistive granite and the conductive structure. The cross-sectional plots of the profiles perpendicular to the DKF and the MCF show that the resistivity contrast corresponding to the DKF at the surface dips southeast with a shallow angle and ends at the MCF (Fig. 7). Unfortunately, the cross-sectional plot parallel to the DKF and the MCF does not clearly show the MJF as in the case of the DKF. For the major MCF, the resistivity contrast near the surface is not distinct as the MCF's surface trace cuts through the high conductivity zones associated with the sedimentary rock and weathered granite rocks filled with fluid (Figs. 6 and 7). However, at depths deeper than 600 m, the resistivity contrast in the north and south of the MCF becomes prominent (Figs. 6e, f and 7). The MCF clearly separates the high resistivity granite rock in the northwest and the moderate resistivity sediments (M) of the Fang basin in the south.

Although there are many high conductivity zones in Fig. 6, here the most interesting feature and the focus of our study is just the C1 and C2 conductors labeled in Figs. 6 and 7. As stated before, there is evidence to link the hot fluid to both conductors. There are three possible major sources for the low resistivity zones shown as C1 and C2 in Fig. 6. The 120 °C water at Fang has a resistivity of 4–8 Ω m as it contains ions dissolved from the rock mineral. When residing in fractures of weathered and altered rocks or sediments, it thus brings down the bulk resistivity of the rocks producing low resistivity zones. Another possible source is the clay-rich rock as interpreted in the other geothermal systems (e.g., Gasperikova et al., 2015; Heise et al., 2008; Rosenkjaer et al., 2015; Uchida and Sasaki, 2006). The third possible interpretation is a combination of both sources.

The C1 conductor is shallow (<100 m depth) and located only beneath the Fang hot spring zone (Figs. 6 and 7). The area beneath C1 was drilled during the 1980s and 1990s from a shallow depth (<100 m) to an intermediate depth (<500 m) (Raksaskulwong, 2011; Thienprasert et al., 1987; Wanakase and Takabut, 1986; Geotermica Italiana SRI, 1984). According to the X-ray diffraction analysis of the cuttings from one well near the hot spring (Ratanasthien et al., 1985), clay content is found intervening with weathered boulders and cataclastic granite at shallow depths (less than 50 m). Unfortunately, no other information about the clay content can be found from the other wells. It is therefore not certain that the low resistivity zone C1 is a result of just the clay-rich rock. Since hot fluid can be extracted from the shallow wells from various depths, one possible interpretation of the C1 is a shallow fracture reservoir trapping the hot fluid within the fractures of altered rock mixed with clay content. The hot fluid from the C1 reservoir then seeps through the surface via the DKF and the MJF. The hot fluid from the C1 reservoir has been used to generate the electricity for many decades.

Another interesting anomaly is the C2 conductor (Figs. 6 and 7) which was not discovered in the past exploration. It is about 1 km south of the Fang hot spring directly below the Huai San Fluorspar Mine (Fig. 6), and just south of the MCF. Unlike C1, the C2 anomaly extends from a shallow depth to a depth of 500 m. At a depth of 200 m, it is roughly 1 km wide. Based on the USGS open report (Shawe, 1984), there are warm water springs (whose temperature was not recorded) found at the bottom of the Huai San Fluorspar Mine, coincidently above the C2 zone. The warm spring is likely to rise along the MCF from a greater depth. Since hot fluid is found in the area, we proposed two possible interpretations for C2.

First, the low resistivity might just be due to the clayey sedimentary rock (Fig. 2) which is part of the Fang basin. This is similar

to the case of the low resistivities found near petroleum exploration wells (Giao et al., 2011). Since hot fluid is found to rise from below, it is possible that this clay-rich semi-consolidate terrace deposit acts as an impermeable zone that traps the hot fluid reservoir directly beneath. This interpretation is basically similar to the caprock concept of the geothermal high temperature magmatic type (e.g., Gasperikova et al., 2015; Heise et al., 2008). According to the Fang conceptual model shown in Fig. 3, conducting an MT survey along the surface, we would expect to "see" the fracture geothermal reservoir as a conductive zone, as with the C1 conductor. Our second interpretation of the C2 conductor is therefore a fracture geothermal reservoir. The hot fluid ascending from deep below is stored in the pores of the sedimentary rock and the fractures of the altered granite beneath before rising to the surface. Whether it is the first or second interpretation, hot fluid residing at depths beneath the C2 anomaly is probably the source of the Fang hot spring. Since the high angle MJF and low angle DKF intersect the MCF in the north of the C2 zone, these local faults act like a passageway for the hot fluid to flow upward to the Fang hot spring as clearly shown in Fig. 7a and b. This is supported by the successful wells located along these faults (Fig. 2) to extract the hot fluid at intermediate depth.

Both interpretations indicate the value of the C2 anomaly as it helps with locating the geothermal reservoir. We therefore need to prove its existence. If the C2 zone fits with the first interpretation, the geothermal reservoir is deep and directly below the C2 anomaly. If it agrees with the second interpretation, the geothermal reservoir is the C2 zone itself which is less depth. Thus the C2 anomaly is possibly an important target for the future drilling location for the geothermal power plant expansion. Drilling over the C2 anomaly will clearly help reveal the geology of Fang geothermal system. We wish to know whether it is a clay-rich semi-consolidate terrace deposit or just a geothermal reservoir. Since the land above C2 lies just outside the Doi Pha Hom Pok national park where the Fang hot spring and the demonstration Fang geothermal power plant are part of, the proposed drilling location above the C2 is possible. In addition, if the fluid rises directly through the MCF from the deep source, its temperature can be expected to be higher than that at the Fang hot spring if it does not mix with the underground water.

5. Conclusion

A geothermal system with potential to generate electricity commercially is the Fang hot spring which currently hosts the only geothermal power plant in Thailand with a power of 0.3MW. The expansion project was halted due to the failure to access a greater flow of hot fluid. In the 2010s, the Fang geothermal project was resumed starting with a magnetotelluric survey. The goal was to gain more understanding about the geothermal system of the Fang hot spring. Thirty-three MT stations covering southern region of the Fang hot spring (northern part is inaccessible as it belongs to the national park) were then installed for 2–3 weeks. A remote site about 600 km south of the study area was also installed during the same period of time to improve the acquired data quality. After the data processing, the data was inverted to produce the 3-D resistivity model.

The obtained 3-D resistivity model is consistent with the geology of the area at the surface. There are many interesting features in the 3-D resistivity model. (1) The high resistive zone R observed in the north of the study area before dipping southward at great depths covers the whole area of study. The high resistivity is consistent with the crystalline granite rocks. It covers a large area and depth. The radiogenic heat from the granite rock may heat the trapped fluid at great depth. Outside of the resistive zone, (2) an intermediate resistive zone (M) is found in the topmost few kilometers. It is interpreted as the Fang sedimentary basin. (3) The resistivity contrast between the high and lower resistivities also matches well with major and minor faults in the area. The resistivity contrasts in the northwest shows that the Doi Kia Fault (DKF) dips southward at a shallow angle and terminates at the major Mae Chan Fault (MCF) in the south. The resistivity contrast between the high resistivity R zone and the intermediate resistivity M zone does not appear until around a depth of 500 m. This contrast is in agreement with the MCF in which the region near the surface was covered with the high conductivity zone.

The focus of this study was mainly on (4) the two conductors: C1 beneath the Fang hot spring and shallow, and C2 about 1 km south of the Fang hot spring and deeper. Based on the evidence of the hot fluid found at the surface, both of them appear related to surface flows of hot water. C1 is a shallow fracture reservoir storing the hot fluid coming from the C2 zone using the DKF and the MJF as a passageway to rise to the surface. C2 is more interesting as it is interpreted as either the clay-rich semi-consolidate terrace deposit on top of the geothermal reservoir or the fracture geothermal reservoir. Either case may be a response to a larger geothermal system that leaked warm water through the MCF at the bottom of the fluorspar mine about 1 km south of the hot springs. The mine is currently filled with drainage water from the power plant and cannot be examined.

Our study is in agreement with the past drilling during 1990s in the vicinity of Fang hot spring above the C1 conductor. The shallow bore holes have been used to draw the hot fluid stored in the C1 conductor to produce electricity for the past few decades. Since C1 has been explored before, this study recommends the exploration and drilling over the C2 conductor which is deeper and might be larger in volume. If C2 is really the geothermal fluid reservoir, the drilled well can be shallow. However, if it is the clay-rich semi-consolidate terrace deposit, drilling may have to be made deeper below the C2 anomaly in order to reach the hot fluid. Both interpretations of the C2 conductor demonstrate that the expansion of the geothermal power plant in the Fang area is possible.

Acknowledgements

The authors would like to thank the Thailand Research Fund (RSA5780010) and the department of groundwater resource (DGR) for the support and permission to publish this study. Mr. Puwis Amatyakul would like to thank the Development and Promotion of Science Talents project (DPST) for a scholarship. We appreciate the technical support during the field work from Mr. Wiboon Kaentao and Miss Rapeeporn Sakulnee of Ensol Co., Ltd. & Panya Consultants Co., Ltd. and Mr. Benchawut Piromfong of Curl-E Geophysics Co., Ltd. We also would like to thank Dr. Kurt Strack and Mr. Tilman Hanstein of KMS technologies – KJT Enterprises Inc. for the MT instruments used in the field survey and technical support, and Dr. Michael Allen for editing the English of this manuscript.

References

Amatyakul, P., Rung-Arunwan, T., Siripunvaraporn, W., 2015. A pilot magnetotelluric survey for geothermal exploration in Mae Chan region, northern Thailand. Geothermics 55, 31–38.

Chaturongkawanich, S., Wongwanich, T., Chuaviroj, S., 1980. Geology of Amphoe Fang, Changwat Chiang Mai Scale 1:15,000. Geological Survey Division. Department of Mineral Resources, Bangkok, Thailand (pp. 49).

Coothongkul, V., Chinapongsanond, P., 1985. Resistivity Survey Fang Geothermal Prospect, Ban Pong Nam Ron. Electricity Generating Authority of Thailand, Amphoe Fang, Chiangmai, Thailand (pp. 61).

Egbert, G.D., 1997. Robust multiple-station magnetotelluric data processing. Geophys. J. Int. 130, 475–496.

Fenton, C.H., Charusiri, P., Wood, S.H., 2003. Recent paleoseismic inverstigations in northern and western Thailand. Ann. Geophys. 46, 957–981.

Gasperikova, E., Rosenkjaer, G.K., Arnason, K., Newman, G. a., Lindsey, N.J., 2015. Resistivity characterization of the Krafla and Hengill geothermal fields through 3D MT inverse modeling. Geothermics 57, 246–257.
Geotermica Italiana SRI, 1984. Geothermal Reconnaissance Survey of Northern Thailand – Final Report. Pisa, Italy, pp. 86 (unplublished report).
Giao, P.H., Doungnoi, K., Senkhamwong, N., Srihiran, S., 2011. Assessment of Petroleum Resources for the South Fang Basin: Uncertainties and Difficulties. Department of Mineral Fuels, Ministry of Energy, Bangkok, Thailand, The 4th Petroleum Forum: Approaching to the 21st Petroleum Concession Bidding Round, May 26–27, 74 p.
Heise, W., Caldwell, T.G., Bibby, H.M., Bannister, S.C., 2008. Three-dimensional modelling of magnetotelluric data from the Rotokawa geothermal field Taupo Volcanic Zone, New Zealand. Geophys. J. Int. 173, 740–750.
IFC-IGA, 2014. Best practices guide for geothermal exploration, 196 p. http://www.ifc.org/wps/wcm/connect/topics_ext_content/ifc_external_corporate_site/ifc+sustainability/learning+and+adapting/knowledge+products/publications/publications_handbook_geothermal-bp-2ed.
Imsamut, S., Krawchan, V., 2005. Geology of Amphoe Fang Quadrangle (4848 IV) and Doi Pha Wok Quadrangle (4748 I), scale 1:50,000: Bureau of Geological Survey. Department of Mineral Resources, Technical Report no BGS 33/2548, 157 p. (in Thai).
Korjedee, T., 2002. Geothermal exploration and development in Thailand. World Geotherm. Congr. 11, 56–66 (2000).
Kosuwan, S., Lumjuan, A., 1998. Neotectonics of Mae Chan Fault in Mae Chan Distrct, Chiang Rai Province Geological Survey Division. Department of Mineral Resources, Bangkok, Thailand.
Lindsey, N.J., Newman, G.A., 2015. Improved workflow for 3D inverse modeling of magnetotelluric data: examples from five geothermal systems. Geothermics 53, 527–532.
Moeck, I.S., 2014. Catalog of geothermal play types based on geologic controls. Renew. Sustain. Energy Rev. 37, 867–882.
Owens, L., 2012. Initial Assessment of High Potential Geothermal Sites in Northern Thailand. Ormat Technologies, Inc., NV, USA, pp. 8 (unpublished report).
Pellerin, L., Johnston, J.M., Hohmann, G.W., 1996. A numerical evaluation of electromagnetic methods in geothermal exploration. Geophysics 61 (1), 121–130.
Praserdvigai, S., 1986. Geothermal development in Thailand. Geothermics 15, 565–582.
Pritchett, J.W., 2004. Finding Hidden Geothermal Resources in the Basin and Range Using Electrical Survey Techniques: a Computational Feasibility Study Report SAIC-04/1031. Science Applications International Corporation, San Diego, CA, USA (202 pp).
Raksaskulwong, M., 2008. Thailand geothermal energy: development history and current status. Proc. 8th Asian Geotherm. Symp., 39–46.
Raksaskulwong, M., 2011. Four decades of geothermal research and development in Thailand. The 9th Asian Geothermal Symposium, 7–9.
Ramingwong, T., Lertsrimongkol, S., Asnachinda, P., Praserdvigai, S., 2000. Update on Thailand geothermal energy research and development. World Geotherm. Congr. 2000 (2), 377–386.
Ratanasthien, B., Panjasawatwong, Y., Yaowanoiyothin, W., Lerdthusnee, S., Haraluck, M., 1985. Water Qualities of Geothermal Fluids from San Kamphaeng and Fang Geothermal Systems. Final Report to Electrical Generating Authority of Thailand (249 p).
Rosenkjaer, G.K., Gasperikova, E., Newman, G.A., Arnason, K., Lindsey, N.J., 2015. Comparison of 3D MT inversions for geothermal exploration: case studies for krafla and hengill geothermal systems in Iceland. Geothermics 57, 258–274.
Shawe, D.R., 1984. Geology and Mineral Deposits of Thailand. Open-File Report. U.S. Geological Survey84–403.
Singharajwarapan, F.S., Wood, S.H., Prommakorn, N., Owens, L., 2012. Northern Thailand geothermal resources and development—a review and 2012 update. Trans. Geotherm. Resour. Counc. 36, 2–6.
Siripunvaraporn, W., Egbert, G., 2009. WSINV3DMT: vertical magnetic field transfer function inversion and parallel implementation. Phys. Earth Planet. Inter. 173, 317–329.
Siripunvaraporn, W., Egbert, G., Lenbury, Y., Uyeshima, M., Ogawa, Y., Junge, A., Jones, A.G., Siripunvaraporn, W., Egbert, G., Lenbury, Y., Uyeshima, M., 2005. Three-dimensional magnetotelluric inversion: data-space method. Phys. Earth Planet. Inter. 150, 3–14.
Takashima, I., Jarach, W., 1987. Isotope geochemistry of six geothermal in northern Thailand. Bull. Geol. Surv. Jpn. 83, 33–40.
Takashima, I., Kawada, K., 1981. Geothermal resources of Thailand, 325. Chishitsu News, pp. 16–29.
Thienprasert, A., Chuaviroj, S., Chaturongkawanich, S., Jaraj, W., Sophonpongpiphat, P., Surinkum, A., Raksaskulwong, M., 1987. Geothermal Energy Resources in Northern Thailand Geothermal Project, Report of Investigation 1. Geological Survey Division. Department of Mineral Resources, Bangkok, Thailand (pp. 208).
Uchida, T., Sasaki, Y., 2006. Stable 3D inversion of MT data and its application to geothermal exploration. Explor. Geophys. 37, 223–230.
Uttamo, W., Elders, C., Nichols, G., 2003. Relationships between Cenozoic strike-slip faulting and basin opening in northern Thailand. Geol. Soc. Lond. Spec. Publ. 210, 89–108.
Wanakasem, S., Takabut, K., 1986. Present status of Fang geothermal project, Thailand. Geothermics 15, 583–587.
Wood, S.H., Singharajwarapan, F.S., 2014. Geothermal systems of Northern Thailand and their association with faults active during the quaternary, in: transactions—Geothermal Resources Council. Geotherm. Resour. Counc., 607–615.